PLANT SCIENCE

Nuclear-localized cyclic nucleotide–gated channels mediate symbiotic calcium oscillations

Myriam Charpentier,[1]* Jongho Sun,[1] Teresa Vaz Martins,[2] Guru V. Radhakrishnan,[1] Kim Findlay,[1] Eleni Soumpourou,[1] Julien Thouin,[3] Anne-Aliénor Véry,[3] Dale Sanders,[4] Richard J. Morris,[2] Giles E. D. Oldroyd[1]*

Nuclear-associated Ca^{2+} oscillations mediate plant responses to beneficial microbial partners—namely, nitrogen-fixing rhizobial bacteria that colonize roots of legumes and arbuscular mycorrhizal fungi that colonize roots of the majority of plant species. A potassium-permeable channel is known to be required for symbiotic Ca^{2+} oscillations, but the calcium channels themselves have been unknown until now. We show that three cyclic nucleotide–gated channels in *Medicago truncatula* are required for nuclear Ca^{2+} oscillations and subsequent symbiotic responses. These cyclic nucleotide–gated channels are located at the nuclear envelope and are permeable to Ca^{2+}. We demonstrate that the cyclic nucleotide–gated channels form a complex with the postassium-permeable channel, which modulates nuclear Ca^{2+} release. These channels, like their counterparts in animal cells, might regulate multiple nuclear Ca^{2+} responses to developmental and environmental conditions.

Nuclear calcium (Ca^{2+}) signals transduce a variety of stimuli in animal (*1*) and plant cells (*2*). Plant genomes lack genes similar to those that encode mammalian nuclear-localized Ca^{2+} channels (*3*), implying that plants have alternative mechanisms for nuclear Ca^{2+} release. Legume root cells show nuclear Ca^{2+} oscillations in response to signaling molecules from nitrogen-fixing rhizobial bacteria and arbuscular mycorrhizal (AM) fungi (*4*). In *Medicago truncatula*, the potassium (K^+)–permeable channel DMI1 (does not make infections 1) and the Ca^{2+}-dependent adenosine triphosphatase (Ca^{2+}-ATPase) MCA8 are necessary for symbiotic Ca^{2+} oscillations; both are located on nuclear membranes, suggesting that the nuclear envelope [contiguous with the endoplasmic reticulum (ER)] acts as the Ca^{2+} store (*5*). Here we identify the Ca^{2+}-permeable channels responsible for Ca^{2+} release from the nuclear envelope–ER stores.

We screened the *M. truncatula* protein database (*6*) to identify transmembrane proteins containing motifs present in Ca^{2+} channels (PF00622, PF02815, PF08763, PF00036, and PF06459), motifs related to ion channels (PF00520, PF07885, PF02386, PF02026, and PF08709), and nuclear localization signal (NLS) motifs (fig. S1A). We assessed their impact on symbioses by silencing the genes that encode these candidates in *M. truncatula* roots. We found that members of the cyclic nucleotide–gated channel (CNGC) family are required for symbiotic associations (fig. S1, B to E). Among the 21 CNGCs of *M. truncatula*, 14 are predicted to contain NLS motifs such as those in DMI1 (*5*) and CASTOR (*7*) (fig. S2), and these fall into CNGC groups II, III, IVA, and IVB (*8*) (fig. S2A).

To differentiate which NLS-containing CNGCs contribute to symbiotic signaling, we used RNA interference to reduce expression of one or several genes from each CNGC group (figs. S3 and S4). Silencing of *CNGC15a, CNGC15b*, and/or *CNGC15c*—all members of group III—correlated with defects in symbiotic associations (Fig. 1A; fig. S3; and fig. S5, A, C, and D). Of the other group III members, *CNGC16* is not expressed in roots (fig. S5B), and silencing *CNGC17* and *CNGC18* did not reduce nodulation (fig. S5, E to J).

We identified mutants in *CNGC14*, *CNGC15a*, *CNGC15b*, and *CNGC15c*, as well as in a CNGC gene that falls outside group III, *CNGC4a*, as a control. One or two insertion alleles were identified for each gene (fig. S6), and these were confirmed to reduce mRNA levels (fig. S6). Nodulation and fungal colonization were assessed in all mutant lines 25 days after inoculation with *Sinorhizobium meliloti* or 5 weeks after inoculation with *Rhizophagus irregularis*. The mutants *cngc15a*, *cngc15b*, and *cngc15c* all showed reduced nodulation and reduced *R. irregularis* colonization (Fig. 1, B and C, and fig. S7, A and B), whereas *cngc4a* and *cngc14* did not. The symbiotic defects of *cngc15* mutants were complemented with their respective genes (Fig. 1, D and E). The mutant lines showed defects in rhizobial infection (Fig. 1F) and induction of early gene expression in response to lipochitooligosaccharide (LCO) signals produced by *S. meliloti* (Nod factor) or *R. irregularis* [nonsulfated (NS)–LCO] (Fig. 1, G and H). We conclude that *CNGC15a, CNGC15b*, and *CNGC15c* function early in the establishment of both rhizobial and mycorrhizal associations.

Oscillations in nuclear Ca^{2+} levels are a feature of the common symbiotic signaling pathway (*9*). The mutants *cngc15a*, *-b*, and *-c*, but not *cngc4a* or *cngc14*, reduced nuclear-associated Ca^{2+} oscillations in response to Nod factor treatment (Fig. 2A and fig. S7C). Fewer cells responded and many cells showed defective Ca^{2+} oscillations in *cngc15* mutants (Fig. 2B), as measured by interspike intervals and probability density functions. Defects included poor maintenance of Ca^{2+} oscillations and irregular oscillation frequencies (Fig. 2, A and B, and fig. S7C). Similar effects were observed after treatments with a mycorrhizal-produced signaling molecule (fig. S8). Nod factor also activates an influx of Ca^{2+} across the plasma membrane, but considering the location of the CNGC15 proteins (discussed below), we do not believe that these proteins will be involved in this Ca^{2+} response. Our data demonstrate that the CNCG15 proteins are required for full activation of nuclear-localized Ca^{2+} oscillations.

We generated double mutants to further assess the function of these channels, but we found equivalent defects to those observed in the single mutants (fig. S7, C to E). Our attempts to generate a triple mutant by crossing *cngc15b-1 cngc15c* with *cngc15a-1 cngc15b-2* or *cngc15a* with *cngc15b-1 cngc15c* were unsuccessful. The efficiency of the crosses, as demonstrated by pod formation, dropped from ~90% (for instance, 9 in 10 crosses of *cngc15a-1* with *cngc15b-2* were successful) to 0% for the generation of the triple mutant (no successful crosses in 103 attempts) (fig. S7F). Fertilization requires coordinated Ca^{2+} signals from the female gametophyte in response to the Ca^{2+} dynamics of the pollen tube (*10*, *11*). *CNGC15a*, *CNGC15b*, and *CNGC15c* are all expressed in flowers and pods (fig. S5B), and *cngc15a* and *cngc15b* had decreased fertilization rates, similar to the double mutants *cngc15b-1 cngc15c* and *cngc15a-1 cngc15b-1* (fig. S9). This suggests a possible function for these channels during fertilization in both female and male gametophytic Ca^{2+} signaling.

Our results demonstrate that CNGC15 proteins support Nod factor– and Myc factor–induced nuclear-localized Ca^{2+} oscillations. We assessed the location of these channels by using functional green fluorescent protein (GFP) fusions (Fig. 1, D and E), analyzed by confocal microscopy and transmission electron microscopy of GFP immunogold–labeled sections (Fig. 3 and figs. S10 and S11A). We found that CNGC15a, CNGC15b, and CNGC15c all localized to the nuclear envelope. We also generated antibodies specific to CNGC15a (fig. S11B), with which we were able to confirm the presence of CNCG15a specifically on nuclear membrane fractions (Fig. 3K). These CNGC proteins and DMI1 have predicted NLS motifs in the N terminus or between the first few transmembrane domains. This is similar to many nuclear membrane–targeted proteins in yeast and animals (*12*); however, additional work is necessary to test the relevance of this positioning of the NLS in plant proteins.

[1]Cell and Developmental Biology, John Innes Centre, Norwich Research Park, Norwich NR4 7UH, UK. [2]Computational and Systems Biology, John Innes Centre, Norwich Research Park, Norwich NR4 7UH, UK. [3]Laboratoire de Biochimie et Physiologie Moléculaire des Plantes, UMR 5004 CNRS–386 INRA (French National Institute for Agricultural Research)–SupAgro-M–Université Montpellier, Campus SupAgro–INRA, 34060 Montpellier, France. [4]Metabolic Biology, John Innes Centre, Norwich Research Park, Norwich NR4 7UH, UK.
*Corresponding authors. Email: myriam.charpentier@jic.ac.uk (M.C.); giles.oldroyd@jic.ac.uk (G.E.D.O.)

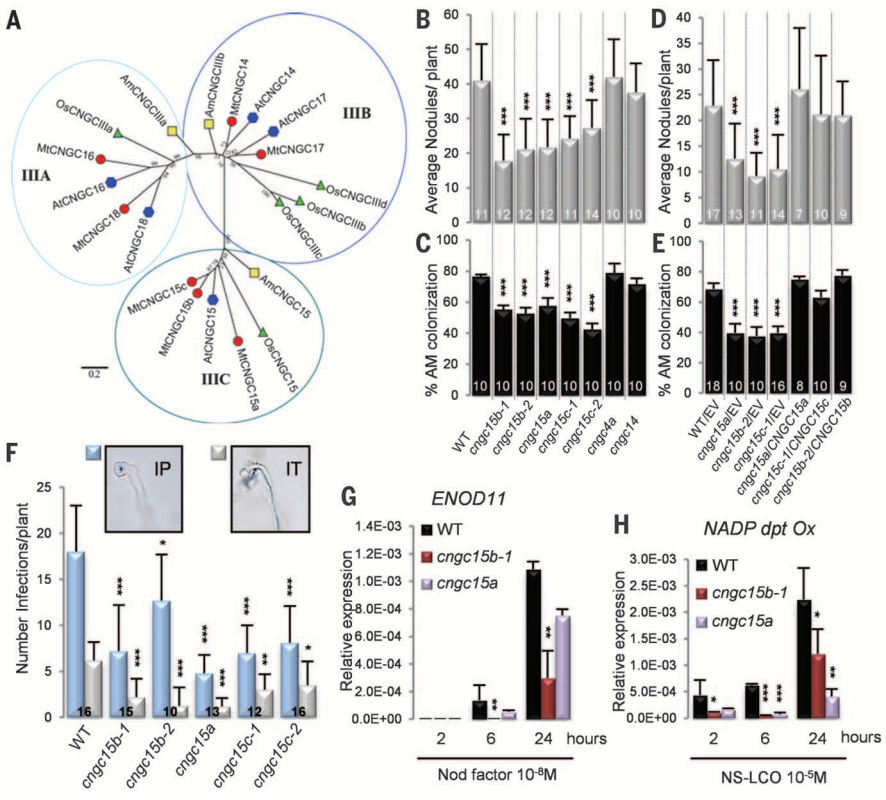

Fig. 1. *CNGC15* gene mutants show symbiotic defects. (**A**) CNGC15a, CNGC15b, and CNGC15c belong to subclass C of the group III CNGCs. The phylogenetic tree includes CNGC group III members from *Amborella trichopoda* (Am, yellow squares), *Oryza sativa* (Os, green triangles), *Arabidopsis thaliana* (At, blue polygons), and *M. truncatula* (Mt, red dots). Numbers at the branch points indicate the percentage bootstrap values (for 1000 iterations) of the consensus tree. (**B**) The *cngc15a*, *-b*, and *-c* mutants were assessed at 25 days after inoculation with *S. meliloti* strain 2011 and (**C**) 5 weeks after inoculation with *R. irregularis* (WT, wild-type *M. truncatula*). (**D**) Complementation of the nodulation and (**E**) mycorrhization phenotypes of *cngc15a*, *-b*, and *-c* by expressing *CNGC15a*, *-b*, and *-c* fused to GFP, driven by the *Lotus japonicus Ubiquitin* promoter (EV, empty vector). (**F**) Infection pockets (IP) and infection threads (IT) were quantified from two biological replicates, 7 days after inoculation with *S. meliloti*. (**G**) Nod factor–induced *ENOD11* expression and (**H**) NS-LCO–induced *NADP dpt Ox* (nicotinamide adenine dinucleotide phosphate–dependent oxidoreductase) expression in WT and *cngc15* mutants after 2, 6, and 24 hours of treatment. Values in (G) and (H) are from three biological replicates each of ten roots, and expression is normalized to that of *EF-1α* (elongation factor 1α). In (B), (D), (F), (G), and (H), error bars show standard deviation. In (C) and (E), error bars show standard error. The number of plants analyzed is given at the bottom of each column. $*P < 0.05$; $**P < 0.01$; $***P < 0.001$ (*t* test).

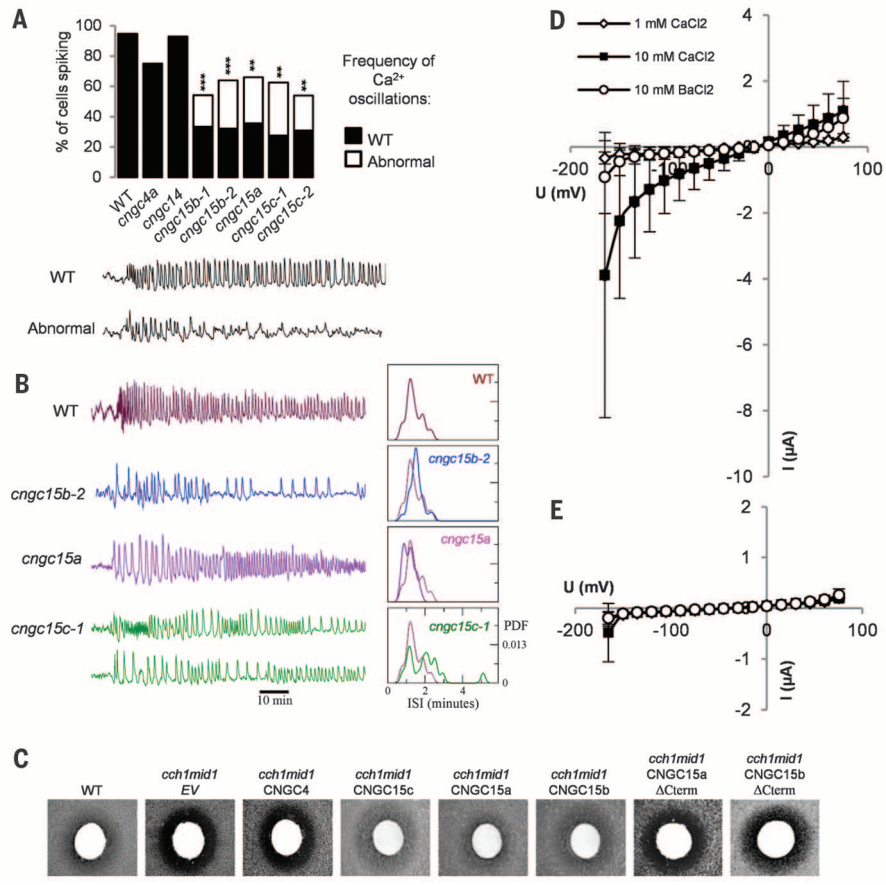

Fig. 2. CNGC15 proteins are required for nuclear Ca^{2+} oscillations and transport Ca^{2+}. (**A**) Nod factor (10^{-9} M)–induced Ca^{2+} spiking, assayed in WT and *cngc* mutants. The number of cells analyzed is shown in fig. S7C. $**P < 0.01$; $***P < 0.001$ (χ^2 test). Below, black traces show examples of calcium traces that were scored as WT or abnormal. (**B**) Representative Ca^{2+} traces of WT roots and mutants, showing detrended Oregon green/Texas red ratios in arbitrary units. The panels on the right show density plots of average interspike intervals (ISI) during 60 min, starting 7 min after the first spike (n = 26 WT, 26 *cngc15b-2*, 24 *cngc15a*, and 17 *cngc15c-1*; PDF, probability density function). (**C**) CNGC15 proteins complement *cch1/mid1*. Discs containing α factor inhibit growth in the mutant but not the WT or *CNGC15*-complemented strains. CNGC15a and CNGC15b with their C termini truncated (ΔCterm) and CNGC4 do not complement *cch1/mid1*. (**D** and **E**) Average current-voltage (*I-U*) relationship in oocytes expressing *CNGC15a* (D) or injected with water (E) in presence of $CaCl_2$ or $BaCl_2$. Error bars represent standard deviation (n = 4).

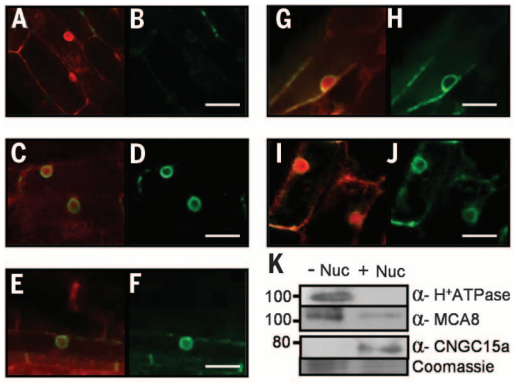

Fig. 3. CNGC15 proteins localize to nuclear membranes. Confocal microscopy of roots expressing the plant marker DsRed alone (**A** and **B**) and with CNGC15b:GFP (**C** and **D**), CNGC15a:GFP (**E** and **F**), CNGC15c:GFP (**G** and **H**), and DMI1:GFP (**I** and **J**) (where the colon denotes fusion). In (A), (C), (E), (G), and (I), the overlay of the green and red channels is shown. In (B), (D), (F), (H), and (J), the green channel is shown. Scale bars, 20 μm. (**K**) The microsomal fraction depleted of nuclei (−Nuc) and the membrane fraction of purified nuclei (+Nuc) from *M. truncatula* roots, assessed with indicated antibodies. Antibodies to H^+ATPase and MCA8 were used as plasma membrane and ER–nuclear membrane markers, respectively. The presence of CNGC15a was detected with its native antibody.

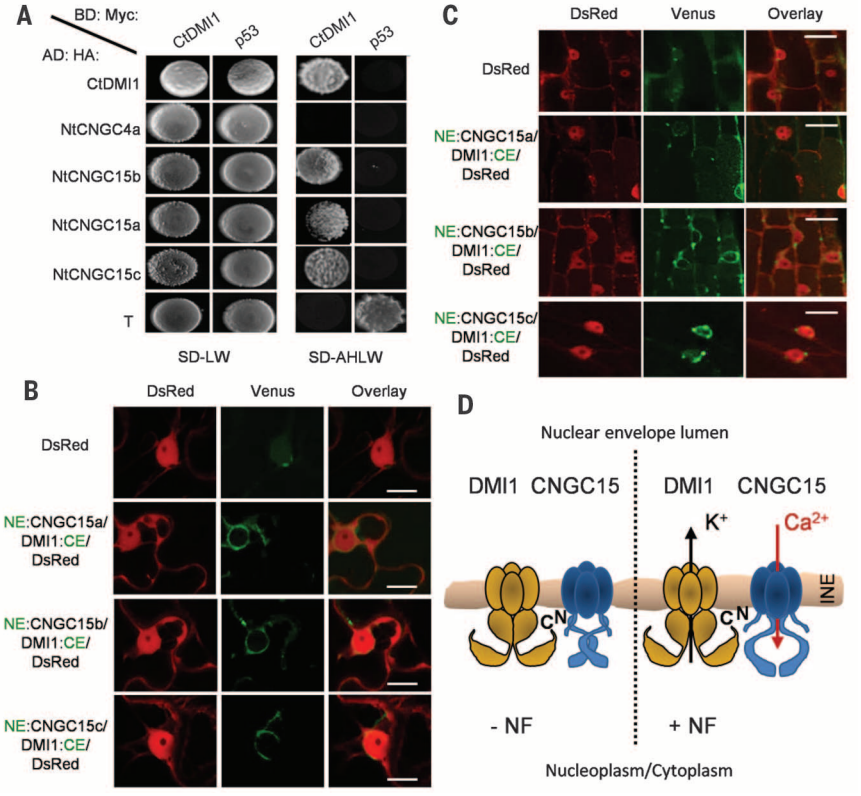

Fig. 4. CNGC15 and DMI1 interact at the nuclear envelope. (**A**) Yeast two-hybrid assays between the C-terminal domain of DMI1 as bait (BD) and the N-terminal domains of CNGC4a, the N-terminal domains of CNGC15 proteins, and the C-terminal domain of DMI1 as prey (AD) (details are given in the supplementary materials). Murine p53 and its interacting partner SV40 large T antigen (simian virus large tumor antigen) were used as a control. SD-LW, synthetic dropout medium lacking Leu and Trp; SD-AHLW, synthetic dropout medium lacking adenine, His, Leu, and Trp. (**B**) *N. benthamiana* leaves transiently expressing N-terminal Venus (NE) fused to the N termini of each CNGC15 and C-terminal Venus (CE) fused to the C terminus of DMI1. DsRed was present in all vectors. Scale bars, 16 μm. (**C**) *M. truncatula* root cells expressing the same fusions. Scale bars, 10 μm. (**D**) A model of CNGC15 and DMI1 dynamics at the inner nuclear envelope (INE). DMI1 interacts physically with CNGC15 to control the simultaneous opening of both channels through direct binding of a secondary messenger to DMI1 or CNGC15 after stimulation with Nod factor (+NF).

To determine whether CNGC15 subgroup members are permeable to Ca^{2+}, we expressed them in the *cch1/mid1* yeast mutant. In response to mating pheromone (α factor), *cch1/mid1* fails to generate cytosolic Ca^{2+} signals, resulting in growth arrest (*13*). This phenotype can be complemented by the release of Ca^{2+} into the cytosol from any Ca^{2+} store. Each of the three CNGC15 proteins was individually able to complement the *cch1/mid1* growth-arrest phenotype (Fig. 2C), suggesting that they are Ca^{2+}-permeable. Additionally, expression of *CNGC15a* in *Xenopus laevis* oocytes triggered an inward Ca^{2+} current (Fig. 2D) that was not observed in control oocytes (Fig. 2E), further demonstrating the Ca^{2+} permeability of this group of channels.

Mathematical modeling has demonstrated that the interplay between the K^+-permeable channel DMI1, a Ca^{2+} channel, and a Ca^{2+}-ATPase can give rise to sustained Ca^{2+} oscillations (*14*). Based on our findings regarding the involvement of CNGC, we adapted this model to introduce a cyclic nucleotide–gating mechanism for the Ca^{2+} channel (*15*) and demonstrated that this system can recapitulate the observed Ca^{2+} oscillations (fig. S12). This model suggests that the activation of DMI1 and CNGC15 must occur simultaneously; introducing lag times in their activation stopped the Ca^{2+} oscillations (fig. S13). One possible mechanism for such simultaneous activation would be the presence of both channels in a single complex. We found that the soluble C terminus of DMI1 and the N termini of CNGC15a, CNGC15b, and CNGC15c interact in yeast (Fig. 4A and fig. S11C). Using bimolecular fluorescence complementation (*16*) of the full-length proteins, we observed interactions at the nuclear envelope between DMI1 and the CNGC15 proteins in both *Nicotiana benthamiana* leaves and *M. truncatula* roots (Fig. 4, B and C); we did not observe interactions in control iterations (fig. S14). Nod factor had no effect on these interactions (fig. S15), implying that the complex is maintained after activation.

We have shown that CNGC15 proteins are responsible for nuclear Ca^{2+} oscillations in the symbiotic signaling pathway of *M. truncatula*. CNGCs have been demonstrated to locate at vacuoles (*17*) or the plasma membrane (*18*). In contrast, CNGC15 proteins are located at the nuclear envelope and are permeable to Ca^{2+}. We propose that the location of these Ca^{2+} channels allows a targeted nuclear release of the ER Ca^{2+} store. Physical interactions between the CNGC15 proteins and DMI1 may support synchronous activation and modulate the Ca^{2+} signal (Fig. 4D). Further work on this nuclear channel complex should clarify how it is regulated and its implication in developmental processes such as fertility.

REFERENCES AND NOTES

1. A. G. Oliveira, E. S. Guimarães, L. M. Andrade, G. B. Menezes, M. Fatima Leite, *Physiology* **29**, 361–368 (2014).
2. N. Pauly *et al.*, *Nature* **405**, 754–755 (2000).
3. G. L. Wheeler, C. Brownlee, *Trends Plant Sci.* **13**, 506–514 (2008).
4. G. E. Oldroyd, *Nat. Rev. Microbiol.* **11**, 252–263 (2013).
5. W. Capoen *et al.*, *Proc. Natl. Acad. Sci. U.S.A.* **108**, 14348–14353 (2011).
6. N. D. Young *et al.*, *Nature* **480**, 520–524 (2011).
7. M. Charpentier *et al.*, *Plant Cell* **20**, 3467–3479 (2008).
8. P. Mäser *et al.*, *Plant Physiol.* **126**, 1646–1667 (2001).
9. R. J. Wais *et al.*, *Proc. Natl. Acad. Sci. U.S.A.* **97**, 13407–13412 (2000).
10. M. Iwano *et al.*, *Development* **139**, 4202–4209 (2012).
11. Y. Hamamura *et al.*, *Nat. Commun.* **5**, 4722 (2014).

12. J. K. Laba, A. Steen, L. M. Veenhoff, *Curr. Opin. Cell Biol.* **28**, 36–45 (2014).
13. M. Fischer *et al.*, *FEBS Lett.* **419**, 259–262 (1997).
14. M. Charpentier, T. Vaz Martins, E. Granqvist, G. E. Oldroyd, R. J. Morris, *Plant Signal. Behav.* **8**, e22894 (2013).
15. D. P. Dougherty, G. A. Wright, A. C. Yew, *Proc. Natl. Acad. Sci. U.S.A.* **102**, 10415–10420 (2005).
16. R. Waadt *et al.*, *Plant J.* **56**, 505–516 (2008).
17. C. C. Yuen, D. A. Christopher, *AoB Plants* **5**, plt012 (2013).
18. T. Borsics, D. Webb, C. Andeme-Ondzighi, L. A. Staehelin, D. A. Christopher, *Planta* **225**, 563–573 (2007).

ACKNOWLEDGMENTS

We thank J.-M. Ané for the construct *35S:DMI1:GFP*, E. Peiter for the *cch1/mid1* mutant, G. Calder for confocal help, E. Barclay for immunogold labeling, P. Bailey for bioinformatics, K. Mysore and J. Wen for *Tnt1* mutant screening, and M. Hopkins for models of CNGC action. The work was supported by the Biotechnology and Biological Sciences Research Council (grants BB/J004553/1 and BB/J018627/1) and by the European Research Council (SYMBIOSIS project). M.C. and G.E.D.O. directed the research. M.C. performed the experiments with contributions by J.S. (calcium spiking), T.V.M. and R.J.M. (mathematical modeling), G.V.R. (phylogeny), K.F. (immunogold labeling and electron microscopy), E.S. (RNA extraction and quantitative reverse transcriptase polymerase chain reaction), and J.T. and A.-A.V. (electrophysiology). M.C., G.E.D.O., and D.S. wrote the manuscript. The supplementary materials contain additional data.

SUPPLEMENTARY MATERIALS

www.sciencemag.org/content/352/6289/1102/suppl/DC1
Materials and Methods
Figs. S1 to S15
Tables S1 to S2
References (*19*–*35*)

7 December 2015; accepted 20 April 2016
10.1126/science.aae0109

METAL ACQUISITION

Biosynthesis of a broad-spectrum nicotianamine-like metallophore in *Staphylococcus aureus*

Ghassan Ghssein,[1,2,3]* Catherine Brutesco,[1,2,3]* Laurent Ouerdane,[4]* Clémentine Fojcik,[5] Amélie Izaute,[1,2,3] Shuanglong Wang,[4] Christine Hajjar,[1,2,3] Ryszard Lobinski,[4] David Lemaire,[2,3,6] Pierre Richaud,[2,3,7] Romé Voulhoux,[8] Akbar Espaillat,[9] Felipe Cava,[9] David Pignol,[1,2,3] Elise Borezée-Durant,[5] Pascal Arnoux[1,2,3]†

Metal acquisition is a vital microbial process in metal-scarce environments, such as inside a host. Using metabolomic exploration, targeted mutagenesis, and biochemical analysis, we discovered an operon in *Staphylococcus aureus* that encodes the different functions required for the biosynthesis and trafficking of a broad-spectrum metallophore related to plant nicotianamine (here called staphylopine). The biosynthesis of staphylopine reveals the association of three enzyme activities: a histidine racemase, an enzyme distantly related to nicotianamine synthase, and a staphylopine dehydrogenase belonging to the DUF2338 family. Staphylopine is involved in nickel, cobalt, zinc, copper, and iron acquisition, depending on the growth conditions. This biosynthetic pathway is conserved across other pathogens, thus underscoring the importance of this metal acquisition strategy in infection.

Metals are required in many life processes, and consequently all organisms have developed mechanisms for their uptake and homeostasis. Pathogenic bacteria must face an additional barrier of metal limitation that is usually set by the host, precisely in order to prevent bacterial growth (*1*). This strategy of "nutritional immunity" by the hosts also extends to many micronutrients with dedicated mechanisms of sequestration for iron, manganese, or zinc (*2*, *3*). The paradigm of metal acquisition in metal-deprived environments is associated with iron: Whereas one strategy consists in transporting the reduced form, the most common scheme involves the synthesis of high-affinity ferric siderophores, their extracellular release before capture, and import of the siderophore-Fe^{3+} complex (*4*). These siderophores are frequently associated with virulence and may also be used for the transport of metals other than iron (*5*, *6*), with only a few examples of other types of microbial metallophores. Methanobactin, for example, is a peptide-based chalkophore used for copper scavenging by methane-oxidizing bacteria (*7*). Free L-histidine (L-His) is used as a nickelophore by some bacteria, and more complex molecules are possibly used by *Staphylococcus aureus* or *Helicobacter pylori*, although their identity or functional relevance are unknown (*8*, *9*). Recently, a nickel/cobalt uptake system (called CntA-F) was uncovered in *S. aureus* and was found to play a role in the virulence of this strain (*10*).

Plants have also evolved their own metal chelators, and among them, nicotianamine is an important metabolite that is essential in the homeostasis of iron, copper, nickel, and zinc (*11*, *12*). Nicotianamine is also the first precursor of phytosiderophores, a family of molecules chemically different from but functionally equivalent to siderophores (*13*). Nicotianamine is enzymatically synthesized by nicotianamine synthase (NAS), which catalyzes the condensation of three α-aminobutyric acid moieties from *S*-adenosylmethionine (SAM) with the cyclization of one of them to form an azetidine ring (*14*–*16*). Nicotianamine and its phytosiderophore derivatives seem to be restricted to plants and some fungi, although some archaea apparently produce a nicotianamine-related molecule called thermonicotianamine, the functional role of which remains unknown (*17*).

Trying to better understand this family of plant NAS and archaeal NAS-like enzymes, we found a gene putatively coding for a NAS-like enzyme in bacterial genomes, including that of *S. aureus*. The NAS-like gene from *S. aureus* (*sav2469*), here called *cntL*, shares 12% sequence identity with one of the four NASs from *Arabidopsis thaliana*, which corresponds to a very distant homology. However, threading-based structure prediction programs detected a structural homology of CntL with eukaryotic NAS and archaeal NAS-like enzymes (fig. S1). The gene coding for CntL is systematically located upstream of a gene whose product belongs to the DUF2338 family (*cntM* in *S. aureus*, *sav2468*; Fig. 1 and fig. S2). Threading-based prediction indicates with high confidence that this family of protein is related to octopine dehydrogenase, a NAD(P)H-dependent enzyme that reductively condensates a free amino acid, such as arginine, with an α-ketoacid, such as pyruvate (*18*). This family of enzymes is known to be involved in the escape of scallops from their starfish predators (*19*) or in the growth of parasitic bacteria, such as *Agrobacterium tumefaciens*, at the expense of plants in which they induce opine-producing tumors, offering bacteria a selective growth advantage (*20*). In *S. aureus*, the gene upstream of *cntL* (*cntK*, *sav2470*) appears restricted to the phylum of Firmicutes and encodes a protein that is distantly related to a diaminopymelate epimerase (DapF).

On the basis of these predictions, the putative activity of each of these three enzymes could be joined together to form a biosynthetic machinery: The CntK epimerase would produce an amine substrate of proper stereochemistry that would be

[1]Laboratoire de Bioénergétique Cellulaire, Institut de Biosciences et Biotechnology Aix-Marseille (BIAM), Commissariat à l'Energie Atomique et aux Energies Alternatives (CEA), 13108 Saint-Paul-lès-Durance, France. [2]UMR 7265, Centre National de Recherche Scientifique, Saint-Paul-lès-Durance, France. [3]Aix Marseille Université, Marseille, France. [4]Université de Pau et des Pays de l'Adour/CNRS, Laboratoire de Chimie Analytique Bio-inorganique et Environnement, IPREM-UMR5254, Hélioparc, 2, Avenue Angot, 64053 Pau, France. [5]Micalis Institute, INRA, AgroParisTech, Université Paris-Saclay, 78350 Jouy-en-Josas, France. [6]Lab Interact Protein Metal, BIAM, CEA, 13108 Saint-Paul-lès-Durance, France. [7]Lab Bioenerget Biotechnol Bacteries et Microalgues, BIAM, CEA, 13108 Saint-Paul-lès-Durance, France. [8]CNRS et Aix-Marseille Université, Laboratoire d'Ingénierie des Systèmes Macromoléculaires (UMR7255), Institut de Microbiologie de la Méditerranée, Marseille, France. [9]Laboratory for Molecular Infection Medicine Sweden, Department of Molecular Biology, Umeå Centre for Microbial Research, Umeå University, Umeå, Sweden.
*These authors contributed equally to this work. †**Corresponding author. Email: pascal.arnoux@cea.fr**

Nuclear-localized cyclic nucleotide–gated channels mediate symbiotic calcium oscillations

Myriam Charpentier, Jongho Sun, Teresa Vaz Martins, Guru V. Radhakrishnan, Kim Findlay, Eleni Soumpourou, Julien Thouin, Anne-Aliénor Véry, Dale Sanders, Richard J. Morris and Giles E. D. Oldroyd

Science **352** (6289), 1102-1105.
DOI: 10.1126/science.aae0109

Calcium signals the making of symbiosis

Plant cell nuclei respond to signals from symbiotic nitrogenfixing rhizobial bacteria or arbuscular mycorrhizal fungi with oscillating Ca^{2+} release. Charpentier *et al.* identified a trio of responsible Ca^{2+} channels in a legume. These channels contain nuclear localization signals and are expressed in root cell nuclear envelopes. The channels function early in the establishment of symbiosis to produce oscillations in Ca^{2+} release from nuclear stores.

Science, this issue p. 1102